whereas the estimated contribution due to measurement uncertainty varied from 6 to 13%. Therefore, these measurements can also be used to estimate the extent of the turbulent fluctuations. In addition, since each temperature measurement is obtained from simultaneous measurements of fluorescence signals from two independent transitions, linear averaging of a series of temperature measurements is permissible; the possible systematic error in the temperature derived from averaged, nonsimultaneous fluorescence measurements is avoided with this technique. With a relatively high data rate (~5 Hz), a well-characterized measurement uncertainty, and the ability to be extended to line imaging, this new instantaneous temperature measurement technique can provide single-pulse measurements in high-temperature reacting flows where temperature, pressure, and species concentrations are subject to turbulence-induced fluctuations.

References

[1]Grinstead, J. H., Laufer, G., and McDaniel, J. C., Jr., "Single-Pulse, Two-Line Temperature Measurement Technique Using KrF Laser-Induced O_2 Fluorescence," *Applied Optics*, Vol. 34, No. 24, 1995, pp. 5501–5512.

[2]Seitzman, J. M., Hanson, R. K., DeBarber, P. A., and Hess, C. F., "Application of Quantitative Two-Line OH Planar Laser-Induced Fluorescence for Temporally Resolved Planar Thermometry in Reacting Flows," *Applied Optics*, Vol. 33, No. 18, 1994, pp. 4000–4012.

[3]McMillin, B. K., Palmer, J. L., and Hanson, R. K., "Temporally Resolved, Two-Line Fluorescence Imaging of NO Temperature in a Transverse Jet in Supersonic Cross Flow," *Applied Optics*, Vol. 32, No. 36, 1993, pp. 7532–7545.

[4]Grinstead, J. H., "Temperature Measurement in High-Temperature Gases Using KrF Laser-Induced O_2 Fluorescence," Ph.D. Dissertation, Dept. of Mechanical, Aerospace, and Nuclear Engineering, Univ. of Virginia, Charlottesville, VA, Jan. 1995.

Multiple-Time-Scale Turbulence Model Computations of Flow over a Square Rib

E. Zeidan* and N. Djilali†
University of Victoria,
Victoria, British Columbia V8W 3P6, Canada

Introduction

TURBULENT flow separation is commonly encountered in both internal and external flows with abrupt changes in geometry. Practical examples of such flows are found in heat exchangers, turbomachinery, combustors, heating and ventilation systems, and cooling of electronic components. The flow over a surface mounted obstacle or rib considered here is related to the classical backward-facing-step geometry but is somewhat more complex because of the formation of multiple primary and secondary recirculation zones and their interaction. The rib geometry provides a good laboratory configuration for further understanding of the physics of flow separation and for evaluating turbulence models and numerical discretization procedures.[1]

The classical two-equation k–ε eddy viscosity model (EVM) and its variants have been the most widely used engineering models to compute separated flows. The performance of these models in separated flows is unsatisfactory in many respects,[2,3] even with the substantial improvements brought about by corrections to account for extra strain effects an streamline curvature.[3,4] One of the weaknesses of EVMs is the use of a single time (or length) scale to characterize the turbulence. This leads to poor predictions of the eddy viscosity in flow situations where large departures from equilibrium conditions occur.

One approach to address this problem is multiscale (MS) turbulence modeling, first proposed by Hanjalić et al.,[5] which consists of partitioning the energy spectrum into several regions, each characterized by a different time scale. In the simplified split-spectrum method used by Kim and Chen,[6] turbulent transport is described by using two time scales: the first corresponds to the large energy-bearing eddies and describes generation of turbulent kinetic energy, and the second corresponds to the smaller-scale eddies and describes dissipation rate. In this Note we examine the performance of Kim and Chen's MS model in high Reynolds number flow over two-dimensional surface-mounted ribs. The computations are performed using a finite volume method with a higher order quadratic upwind scheme, which is stable and conservative and which incorporates an upstream-weighted curvature correction.

Turbulence Model

To account for the evolution of the different scales in the large-eddy production range and the small-eddy dissipation range, the turbulent energy spectrum can be partitioned into three regions:

1) Production region, characterized by the turbulent kinetic energy k_p and the energy transfer rate ε_p.

2) Transfer region, characterized by the turbulent kinetic energy k_t and the dissipation rate ε_t.

3) Dissipation region, where the turbulent kinetic energy is dissipated into heat.

Kim and Chen's MS turbulence model formulation[6] used in this study is based on a single-point closure with a variable spectrum-partitioning method. The location of the partition, or the ratio k_p/k_t, is determined as part of the solution and is dependent on the turbulence intensity, production, transfer, and dissipation rates. The partition is moved toward the high-wave number region when production is high and towards the low-wave number region when production is low. Turbulent transport is described by using a time scale characterizing large eddies, and the dissipation rate is characterized by using the fine-scale eddies.

The turbulent kinetic energy and the energy transfer rate equations for the energy containing large eddies are given by[6]

$$\frac{\partial(\rho U_i k_p)}{\partial x_i} - \frac{\partial}{\partial x_i}\left\{\left(\mu + \frac{\mu_t}{\sigma_{k_p}}\right)\frac{\partial k_p}{\partial x_i}\right\} = \rho G_k - \rho\varepsilon_p \tag{1}$$

$$\frac{\partial(\rho U_i \varepsilon_p)}{\partial x_i} - \frac{\partial}{\partial x_i}\left\{\left(\mu + \frac{\mu_t}{\sigma_{\varepsilon_p}}\right)\frac{\partial \varepsilon_p}{\partial x_i}\right\} = C_{p1}\frac{\rho G_k^2}{k_p} + C_{p2}\frac{\rho G_k \varepsilon_p}{k_p} - C_{p3}\frac{\rho \varepsilon_p^2}{k_p} \tag{2}$$

The turbulent kinetic energy and dissipation rate equations for the fine-scale eddies are given by

$$\frac{\partial(\rho U_i k_t)}{\partial x_i} - \frac{\partial}{\partial x_i}\left\{\left(\mu + \frac{\mu_t}{\sigma_{k_t}}\right)\frac{\partial k_t}{\partial x_i}\right\} = \rho\varepsilon_p - \rho\varepsilon_t \tag{3}$$

$$\frac{\partial(\rho U_i \varepsilon_t)}{\partial x_i} - \frac{\partial}{\partial x_i}\left\{\left(\mu + \frac{\mu_t}{\sigma_{\varepsilon_t}}\right)\frac{\partial \varepsilon_t}{\partial x_i}\right\} = C_{t1}\frac{\rho \varepsilon_p^2}{k_t} + C_{t2}\frac{\rho\varepsilon_p\varepsilon_t}{k_t} - C_{t3}\frac{\rho\varepsilon_t^2}{k_t} \tag{4}$$

where the production rate is given as

$$G_k = \frac{\mu_t}{\rho}\left\{2\left(\frac{\partial U}{\partial x}\right)^2 + 2\left(\frac{\partial V}{\partial y}\right)^2 + \left(\frac{\partial U}{\partial y} + \frac{\partial V}{\partial x}\right)^2\right\}$$

and the empirical coefficients are determined by examining limiting cases of asymptotic turbulence growth and decay rates and

Received April 5, 1995; revision received Oct. 17, 1995; accepted for publication Oct. 18, 1995.

*Graduate Research Assistant, Department of Mechanical Engineering.

†Associate Professor, Department of Mechanical Engineering. Member AIAA.

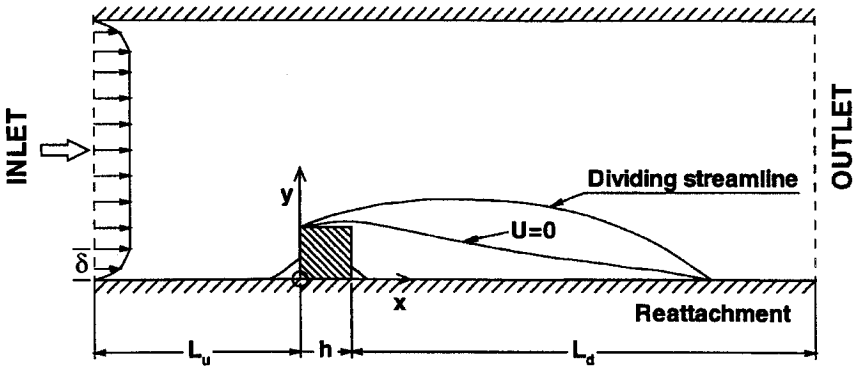

Fig. 1 Geometry of the flow over a surface-mounted rib.

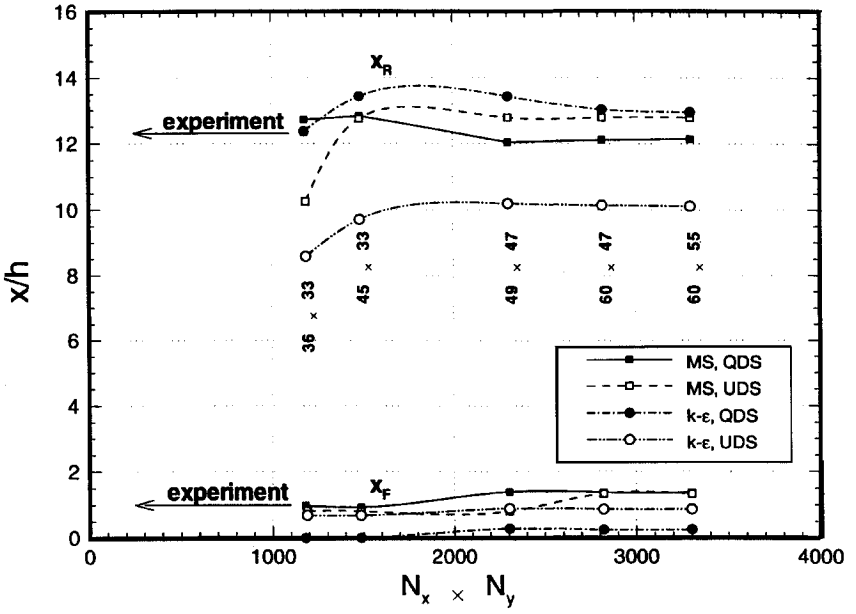

Fig. 2 Effect of grid refinement on computed lengths of the upstream and downstream separation bubbles.

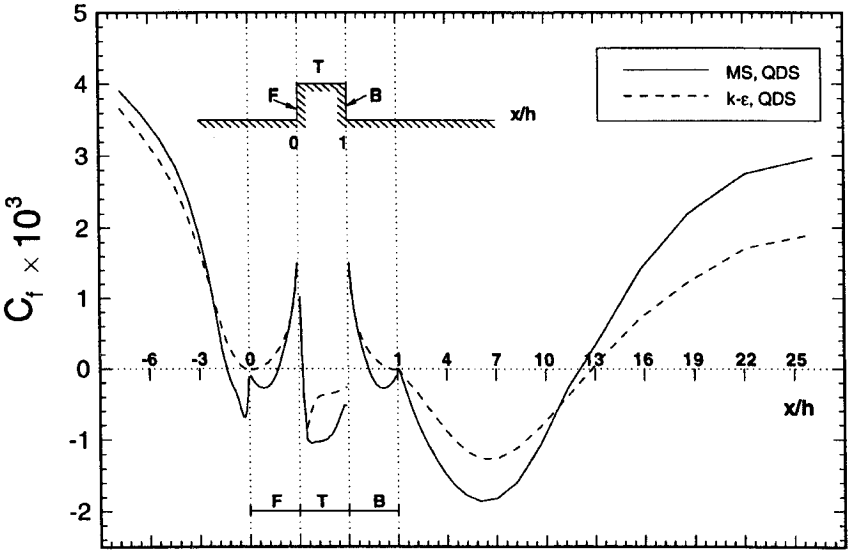

Fig. 3 Wall shear stress distribution.

equilibrium turbulence conditions. Further details are given in Refs. 6 and 7.

Once the turbulent kinetic energy $k = k_t + k_p$, and the dissipation rate ε_p are computed, the eddy viscosity is determined using the Prandtl–Kolmogorov relation $\mu_t = C_\mu \rho(k^2/\varepsilon_p)$. This expression is similar to that used in the single-scale k–ε model except that the dissipation is replaced by the energy transfer rate. In effect, this implies that the turbulence length scale is related to the energy transfer rate of the large, energy-bearing eddies rather than to the dissipation rate.

Computational Procedure

The geometry of the computational domain is shown in Fig. 1. The blockage ratio (rib height/channel width) of the square rib is 7.8%. The inlet section is located at $10h$ upstream of the rib, and the outlet section is located at about $30h$ downstream. A one-seventh

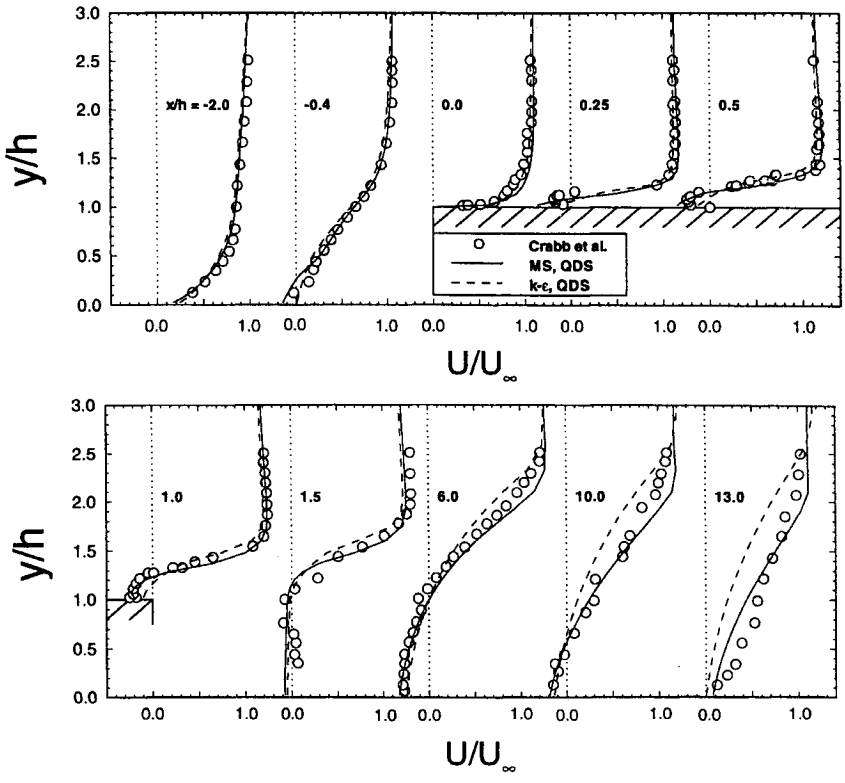

Fig. 4 Computed and measured longitudinal velocity profiles.

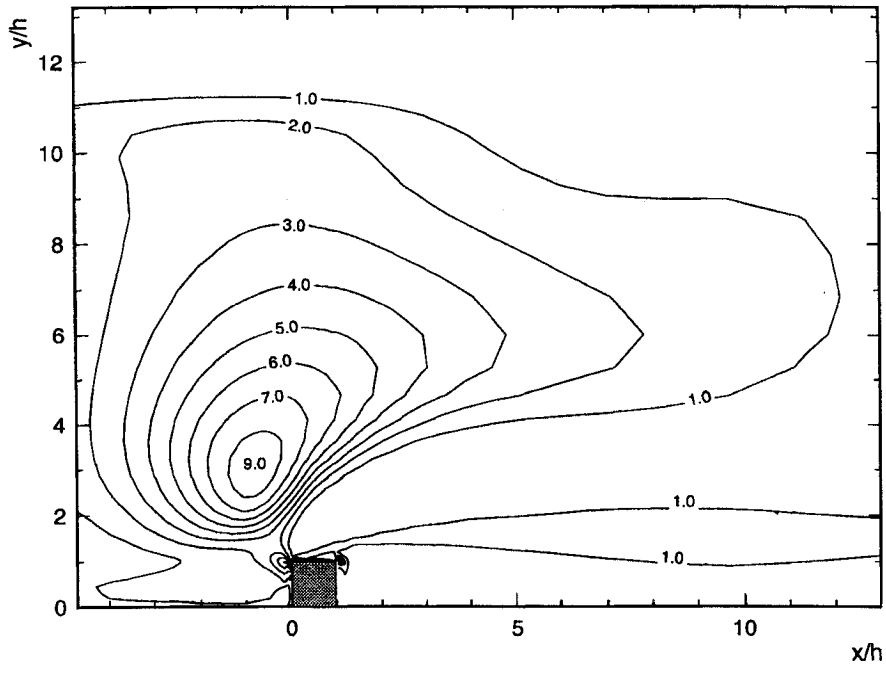

Fig. 5 Contours of the ratio of turbulent kinetic energy production to dissipation rates (MS/QDS).

power-law boundary layer velocity profile is imposed at the inlet plane with a boundary layer thickness of $0.5h$ to simulate the experiment of Crabb et al.[8] A zero-gradient condition is imposed at the outlet section. No-slip boundary conditions with wall functions are imposed along solid walls. The ratios of k_p/k_t and $\varepsilon_t/\varepsilon_p$ at the inlet and along solid walls are based on the computational results of the fully developed channel flow and near wall analysis, respectively.

Equations (1–4) together with the Reynolds averaged Navier–Stokes equations are discretized by a finite volume technique with a staggered, nonuniform grid arrangement. A third-order accurate quick scheme, incorporating a transverse curvature correction,[9] is used to discretize the convective terms. A deferred correction formulation is adopted to ensure boundedness and to maintain a tridiagonal structure of the coefficient matrix. The turbulence model and discretization scheme were implemented by modifying the TEMA code.[10] A more detailed description of the numerical procedure can be found in Ref. 7.

Results and Discussion

Two important characteristic length scales of the rib flow are the upstream and downstream separation bubble lengths. The grid sensitivity of the solution was assessed by monitoring the predicted reattachment length of the main recirculation zones. The results are shown in Fig. 2 using both the k–ε and the MS turbulence models with the first-order upwind differencing scheme (UDS) and the quick differencing scheme (QDS). The k–ε/UDS computations

unpredicted the experimental reattachment length ($x_r/h = 12.3$) by about 15% owing to the combined effect of inadequacies of the k–ε model and numerical diffusion associated with UDS in such flows.[2–4] In the backward-facing step[11] and the bluff plate[4] cases, k–ε predictions are improved by invoking higher order schemes but still yield reattachment lengths shorter than experimental values. In contrast, in the rib flow considered here k–ε/QDS computations overpredict the reattachment length by about 8%, as shown in Fig. 2. The better agreement in this case is fortuitous and is the result of the more complex flow associated with the presence of two primary separation bubbles. The underpredicted upstream separation bubble causes an underretarded flow immediately upstream of the second separation. This results in artificially higher momentum fluxes in the shear layer separating from the upstream edge, thereby compensating for the overdiffusive properties of the k–ε model; the net effect is an overpredicted reattachment length. The values predicted by the MS turbulence model with QDS converge to within 1% of the experimental value. A small secondary recirculation zone behind the rib is obtained with the fine grid QDS computations.

Various flow zones can be identified in the wall shear stress distributions presented in Fig. 3. The distributions obtained from the k–ε and MS models show significant differences on top of and downstream from the rib. The upstream separation region is almost nonexistent in the k–ε predictions, and the magnitudes of the shear stress are lower than those of the MS model because of the over diffusive properties of the k–ε model.

The predicted longitudinal velocity profiles are compared in Fig. 4 to available measurements. The upstream profiles (at $x/h = -2.0$) are almost identical for both models and show a distribution similar to that of fully developed turbulent flow. At $x/h = -0.4$, the effect of the adverse pressure gradients caused by the obstacle becomes more prominent and the two models start deviating noticeably, with the MS model showing better agreement with measurements. The maximum reverse velocity shortly after separation on the top surface of the rib ($x/h = 0.25$) is overestimated by the MS turbulence model, while the zero mean velocity line passes through $0.23h$ above the trailing edge of the rib compared to the experimental value of $0.3h$. Overall, improved predictions with the MS model are obtained throughout. However, the first profile in the recovery zone ($x/h = 13$), though better predicted by the MS turbulence model, is not entirely satisfactory. The excessive retardation of the boundary layer in the recovery region is a discrepancy common to all available EVM and Reynolds stress model computations of reattaching flows.

An important parameter in the MS model is the turbulent kinetic energy generation-to-dissipation ratio (G_k/ε_t). This ratio determines the location of the variable partitioning of the energy spectrum, which is central to the capabilities of the MS model in resolving nonequilibrium fields. The computed contour lines of the ratio G_k/ε_t in Fig. 5 show peak nonequilibrium state associated with large turbulent kinetic energy production around the upstream edge of the rib. The ability of the MS model to resolve turbulence dynamics in this region yields less damping and hence improved predictions of the downstream flow.

Acknowledgments

The financial support of the Natural Sciences and Engineering Research Council of Canada (Grant OGP0105723) and the University of Victoria is gratefully acknowledged.

References

[1]Kessler, R., Perić, M., and Sheuerer, G., "Solution Error Estimation in Numerical Prediction of Turbulent Recirculating Flows," *Validation of Computational Fluid Dynamics*, AGARD CP 437, 1988, pp. 9.1–9.12.

[2]Bergeles, G., and Athanassiadis, N., "Numerical Study of the Flow Around a Surface-Mounted Prism," *Proceedings of Symposium on Refined Modelling of Flows* (Paris, France), 1982, pp. 47–57.

[3]Benodekar, R. W., Goddard, A. G. H., Gosman, A. D., and Issa, R. I., "Numerical Prediction of Turbulent Flow over Surface-Mounted Ribs," *AIAA Journal*, Vol. 23, No. 3, 1985, pp. 359–366.

[4]Djilali, N., Gartshore, I. S., and Salcudean, M., "Turbulent Flow Around a Bluff Rectangular Plate, Part II: Numerical Predictions," *Journal of Fluids Engineering*, Vol. 113, 1991, pp. 60–67.

[5]Hanjalić, K., Launder, B. E., and Schiestel, R., "Multiple-Time-Scale in Turbulence Transport Modeling," *Turbulent Shear Flows 2*, Springer–Verlag, Berlin, 1980, pp. 36–49.

[6]Kim, S.-W., and Chen, C. P., "A Multiple-Time-Scale Turbulence Model Based on Variable Partitioning of the Turbulent Kinetic Energy Spectrum," *Numerical Heat Transfer B*, Vol. 16, 1989, pp. 193–211.

[7]Zeidan, E., Ph.D. Thesis, Dept. of Mechanical Engineering, Univ. of Victoria, BC, Canada, 1995.

[8]Crabb, D., Durão, D. F. G., and Whitelaw, J. H., "Velocity Characteristics in the Vicinity of a Two-Dimensional Rib," *Proceedings of the 4th Brazilian Congress of Mechanical Engineering* (Florianopolis, Brazil), 1977, pp. 415–428.

[9]Leonard, B. P., "Elliptic Systems: Finite Difference Method IV," *Handbook of Numerical Heat Transfer*, Wiley, New York, 1988, pp. 347–378.

[10]Lai, K. Y. M., and Salcudean, M., Internal Rept., Dept. of Mechanical Engineering, Univ. of Ottawa, ON, Canada, 1985.

[11]Lein, F. S., and Leschziner, M. A., "Upstream Monotonic Interpolation for Scalar Transport with Application to Complex Turbulent Flows," *International Journal for Numerical Methods in Fluids*, Vol. 19, 1994, pp. 527–548

Comparison of Baldwin–Lomax Turbulence Models for Two-Dimensional Open Cavity Computations

Chung-Jen Tam,* Paul D. Orkwis,†
and
Peter J. Disimile‡
University of Cincinnati, Cincinnati, Ohio 45221-0070

Introduction

THE presence of a cavity in a surface bounding a fluid flow can cause large pressure, velocity, and density fluctuations in its vicinity, as well as propagating acoustic waves. In addition, the drag on the surface can be altered and structural failure due to resonance can occur. A persistent problem with the numerical simulation of cavity flow is the choice of an appropriate turbulence model. Many researchers have opted for the simplicity of the Baldwin–Lomax algebraic model, although many modifications to its basic form have been employed. Suhs[1] applied the standard Baldwin–Lomax model above the up- and downstream flat plates and bottom wall of the cavity, while assuming laminar flow in the region above the cavity. Rizzetta[2] used the Baldwin–Lomax model with the relaxation model[3] for three-dimensional supersonic open cavity flows. Baysal et al.[4] have researched supersonic open cavity flows using the Baldwin–Lomax turbulence model and a combination of the relaxation modification, the Degani and Schiff[5] first peak modification, and the multiple-wall modification.

Although many turbulence model modifications for cavity flowfields have been proposed, little evidence has been offered as to the suitability of a particular choice. Time-averaged surface pressure data appear to agree quite well for all models but, apparently, different flowfield behavior has been reported. This Note presents the numerical results[6] of a two-dimensional open cavity flowfield study that employed the double thin-layer Navier–Stokes equations and various versions of the Baldwin–Lomax algebraic turbulence models, including the upstream relaxation,[2,4] first peak,[4] multiple-wall,[4]

Presented as Paper 95-0361 at the AIAA 33rd Aerospace Sciences Meeting, Reno, NV, Jan. 11–14, 1995; received Jan. 30, 1995; revision received April 24, 1995; accepted for publication May 18, 1995.

*Research Assistant. Member AIAA.

†Assistant Professor of Aerospace Engineering and Engineering Mechanics. Senior Member AIAA.

‡Associate Professor of Aerospace Engineering and Engineering Mechanics. Member AIAA.